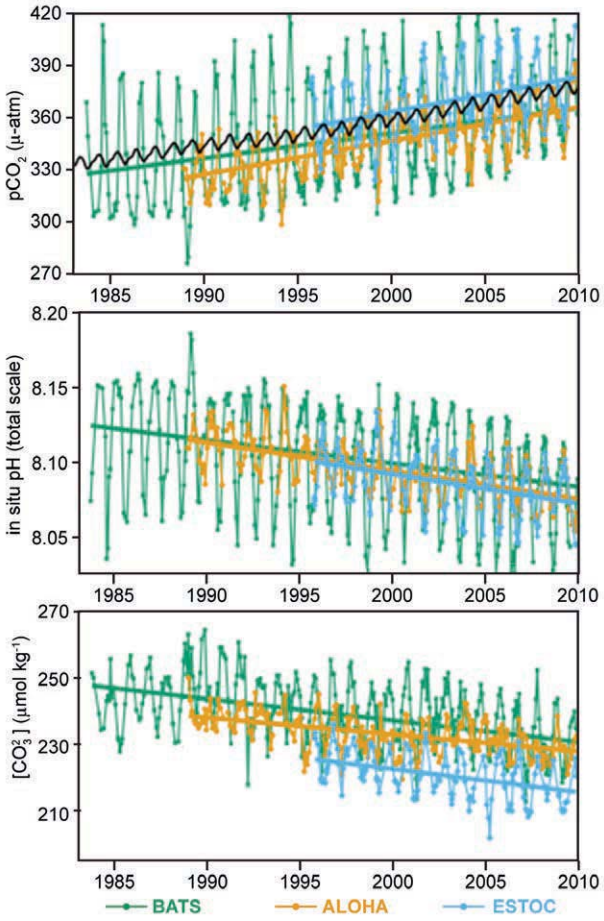

Fig. 3.32. Long-term trends of (top) surface seawater pCO_2, (middle) pH, and (bottom) carbonate ion concentration at three subtropical ocean time series in the North Atlantic and North Pacific Oceans, including: Bermuda Atlantic Time-series Study (BATS, 31°40'N, 64°10'W; green) and Hydrostation S (32°10'N, 64°30'W) from 1983 to present (published and updated from Bates 2007); Hawaii Ocean Time-series (HOT) at Station ALOHA (A Long-term Oligotrophic Habitat Assessment; 22°45'N, 158°00'W; orange) from 1988 to present (published and updated from Dore et al. 2009); and European Station for Time series in the Ocean (ESTOC, 29°10'N, 15°30'W; blue) from 1994 to present (published and updated from González-Dávila et al. 2010). Atmospheric pCO_2 (black) from Hawaii is shown in the top panel. Lines show linear fits to the data (after Orr 2011).

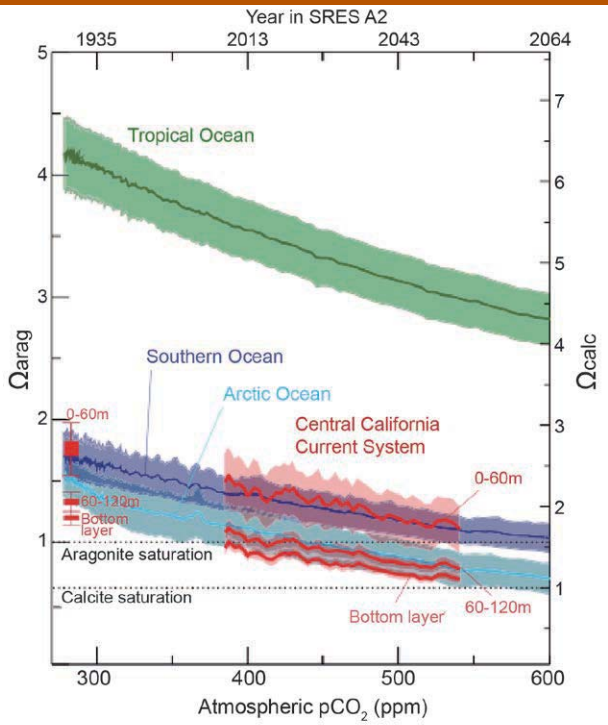

Fig. 3.33. Temporal changes of the average saturation state for aragonite (left y-axis) and calcite (right y-axis) in the nearshore region of the California Current system as function of atmospheric CO_2. For the California Current system three depth ranges are shown; 0–60 m, 60 m–120 m, and the bottom layer above the sediments. Also shown are the saturation states for surface waters of the tropical ocean, Southern Ocean, and Arctic Ocean for comparison (after Gruber et al. 2012).

Recent models have suggested that waters that are undersaturated with respect to aragonite, a carbonate mineral, would shoal to depths affecting the Washington-Oregon-California continental shelf ecosystems over the next several decades (Hauri et al. 2009; Rykaczewski and Dunne 2010; Gruber et al. 2012; Hauri et al. 2013). Figure 3.33 shows the decrease in aragonite saturation levels as a function of atmospheric CO_2 concentrations for surface waters of the tropical, Southern, and Arctic Oceans, and the California Current system (Gruber et al. 2012). The subsurface waters of the California Current system (60-m–120-m depth) reach undersaturation at about the same atmospheric CO_2 concentration as the Arctic Ocean surface waters (~440 μatm). Under these conditions, more than half of the waters of the California Current system would be undersaturated year-round. These large-scale changes would have major implications for shellfish.

4) Global ocean phytoplankton—B. A. Franz, M. J. Behrenfeld, D. A. Siegel, and P. J. Werdell

Marine phytoplankton are responsible for roughly half the net primary production (NPP) on Earth, fixing atmospheric CO_2 into food that fuels global ocean ecosystems and drives the ocean's biogeochemical cycles. Phytoplankton distributions are highly sensitive to environmental changes such as increased ocean temperatures that stratify the water column and prohibit the transfer of cold, nutrient rich waters

to the upper ocean euphotic zone. The global distribution of phytoplankton populations is highly variable, thus requiring satellite observations to provide sufficient frequency and perspective to monitor changes. Satellite ocean color sensors such as Sea-viewing Wide Field-of-view Sensor (SeaWiFS; McClain 2009) and Moderate Resolution Imaging Spectroradiometer (MODIS; Esaias et al. 1998) retrieve the spectral distribution of visible solar radiation reflected upward from beneath the ocean surface. Spectral variations in ocean color (water-leaving reflectance) relate to changes in the phytoplankton pigment chlorophyll-*a* (Chl*a*; mg m^{-3}), yielding a rough satellite-based proxy for phytoplankton abundance. Combined, SeaWiFS (1997–2010) and MODIS on Aqua (MODISA; 2002–present) provide a continuous 16-year record of global ocean color measurements, and the recently launched Visible and Infrared Imaging Radiometer Suite (VIIRS; 2011–present) is now under evaluation as a potential source for continuity of climate-quality Chl*a* data in the coming years (Turpie et al. 2012).

Annual mean Chl*a* from MODISA and VIIRS for 2012 were derived by NASA using consistent processing algorithms (OBPG 2013; Fig. 3.34). Chl*a* concentrations are spatially heterogeneous and range over three orders of magnitude, from <0.05 mg m^{-3} in central ocean gyres to >50 mg m^{-3} in nutrient-rich coastal and subpolar waters. Over the full range of deep-ocean values (>1-km depth), a significant correlation exists between the 2012 annual averages from MODISA and VIIRS in $\log_{10}$(Chl*a*) ($R^2 = 0.96$, $p << 0.001$), thus providing independent confirmation of the large-scale distribution.

Monthly climatological average Chl*a* values were calculated from nine years of MODISA measurements (2003–11) and subtracted from monthly values for each year (Fig. 3.35). As in previous *State of the Climate* reports (e.g., Siegel et al. 2012), the anomaly analyses indicate a general inverse correlation between chlorophyll and similarly-derived SST anomalies (not shown). A warming sea surface layer often associates with shallower mixing depths, reduced vertical nutrient transport, and higher average light levels in the mixed layer, which together drive decreases in chlorophyll concentration (Behrenfeld et al. 2006). In 2012, the large increases in Chl*a* in the tropical Pacific surrounding an equatorial decrease correspond to increased equatorial SST surrounded by cooler tropical waters. Likewise, decreased Chl*a* in the subtropical and increased Chl*a* in the eastern subarctic Atlantic correspond to an inverse pattern in SST. Chl*a* changes in the equatorial and subtropical

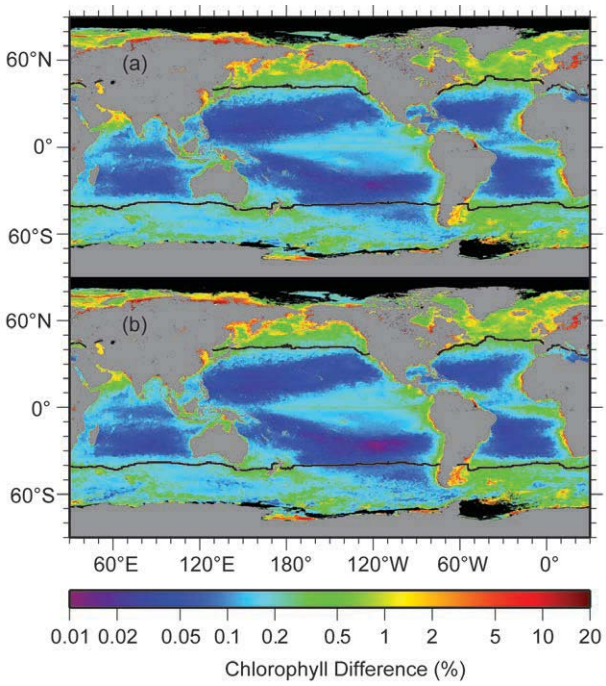

Fig. 3.34. Annual mean Chl*a* distribution derived from (a) MODIS Aqua and (b) VIIRS for 2012. Also shown is the location of the mean 15°C SST isotherm (black lines) that delineates the permanently stratified warm ocean. Chl*a* measurements are taken from NASA Reprocessing of MODISA (version 2012.0) and VIIRS (version 2012.2), averaged into geo-referenced equal area bins of approximately 9.2 × 9.2 km² (Campbell et al. 1995) and mapped to an equirectangular projection centered at 150°W.

Atlantic also follow a generally inverse relationship with SST changes. Also consistent with the earlier reports, the correspondence between chlorophyll and SST anomalies in 2012 breaks down in certain regions, particularly in the subtropical south Indian and eastern subarctic Pacific Oceans.

The black lines in Fig. 3.35 delineate the permanently stratified ocean (PSO), which extends latitudinally between approximately 40°N and 40°S, occupies ~74% of the global ocean surface area, maintains annual average surface temperatures >15°C, and remains perpetually depleted in surface nutrients (Behrenfeld et al. 2006). Figure 3.36 shows the multimission record of monthly mean Chl*a* and monthly anomalies for the PSO, starting with the SeaWiFS mission and extending into the MODISA and VIIRS eras (OBPG 2013). Also shown is the multivariate ENSO index (MEI; Wolter and Timlin 1998), which partially explains the variability in phytoplankton NPP for the PSO for the first eight years of the SeaWiFS mission (Behrenfeld et al. 2006). With some exceptions, the MEI continues to track large-

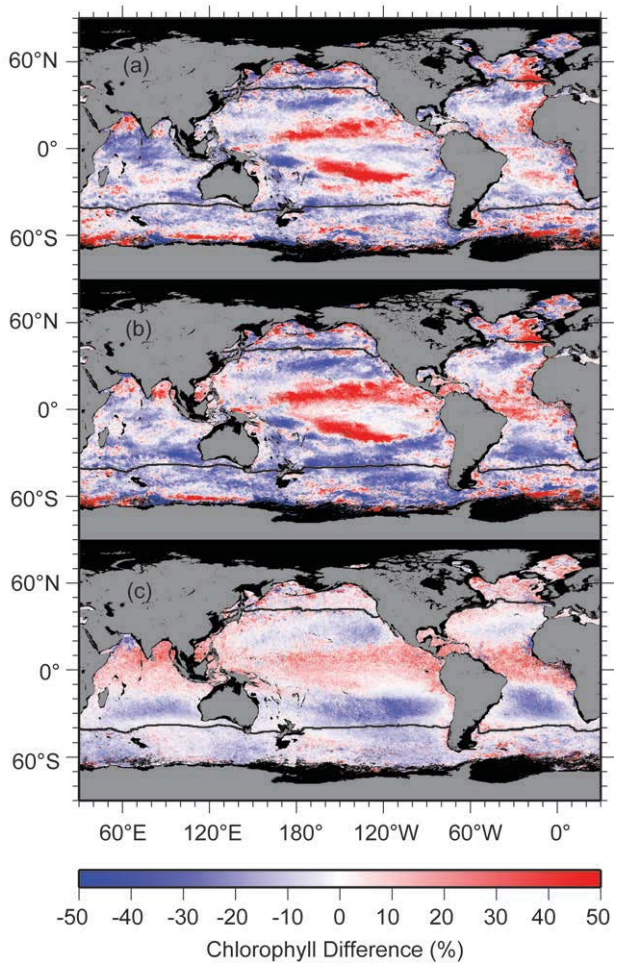

Fig. 3.35. Spatial distribution of summed monthly Chl*a* anomalies for (a) MODIS and (b) VIIRS, where monthly differences were derived relative to the 9-year monthly climatology of MODISA (2003–11), expressed as % difference relative to the climatology, and averaged over 2012. Panel (c) shows the difference between the MODISA and VIIRS anomaly images. Also shown in each panel is the location of the mean 15°C SST isotherm (black lines) delineates the permanently stratified ocean (PSO).

scale PSO temporal variability over the multimission Chl*a* record. A strong El Niño to La Niña transition occurred in 2010, with commensurate reduction in stratification of the tropical Pacific that is clearly reflected by a rapid increase in the Chl*a* anomaly trend (Fig. 3.35a,b). After 2010, correlation between PSO Chl*a* anomalies and MEI is less clear, but this deviation from the long-term pattern may be indicative of increased uncertainty in sensor calibration rather than a fundamental change in the functioning of the ocean biology-climate system.

Globally, for 2012, the MODISA and VIIRS Chl*a* anomalies exhibit a strong correspondence (Figs. 3.35a,b; $R^2 = 0.66$, $p << 0.001$), thus adding confirmation to the large-scale anomaly patterns; and the VIIRS Chl*a* record shows good agreement with MODISA for the PSO, with mean absolute difference in monthly anomalies of 2.4% (Fig. 3.36), suggesting that the consistently-processed VIIRS record may well be able to extend the Chl*a* time series at a level of quality consistent with MODISA. There are, however, significant regional differences in annual anomalies for the two missions (Fig. 3.35c) that provide an indication of uncertainty and raise questions about whether existing technologies will be able to accurately detect the subtle variations in ocean phytoplankton that may be associated with long-term climate change. The goal is to resolve long-term trends in Chl*a* anomalies with a precision approaching 0.1% per year (Siegel and Franz 2010; Siegel et al. 2013). When averaged over all deep-water locations, the annual Chl*a* anomalies for MODISA and VIIRS agree to within 1%, but with a standard deviation of ±30%. These relatively large regional differences are due in part to calibration errors that will likely be reduced in subsequent repro-

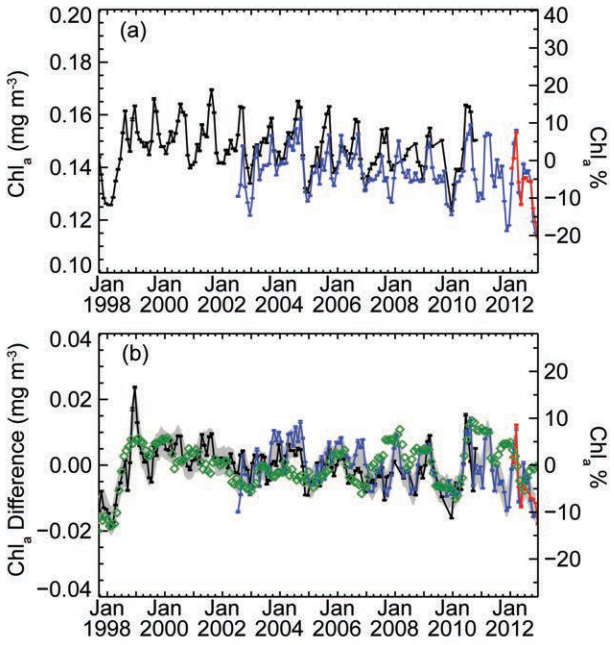

Fig. 3.36. Long-term (15-year) multimission record of Chl*a* averaged over the permanently stratified ocean for SeaWiFS (black), MODISA (blue), and VIIRS (red). (a) shows the independent record from each mission and (b) shows the monthly anomaly after subtraction of the monthly climatological mean (SeaWiFS relative to SeaWiFS climatology, MODISA and VIIRS relative to MODISA climatology). The gray region in (b) shows the averaged difference between SeaWiFS and MODISA over the common mission lifetime. Green diamonds show the Multivariate ENSO Index, inverted and scaled to match the range of the Chl*a* anomalies.

cessing: VIIRS is a new instrument and its calibration is not yet well understood, while MODISA is an aging instrument and its calibration is increasingly challenging (Turpie et al. 2012; Meister et al. 2012). However, both VIIRS and MODISA suffer from several design choices that reduce accuracy for ocean color science relative to SeaWiFS, including reduced spectral coverage in the green leading to degraded accuracy of Chl*a* retrievals in coastal waters, lack of tilting capabilities that results in reduced sampling due to Sun glint contamination (specular reflection from the surface), and significant sensitivity to atmospheric polarization that increases complexity and uncertainty in modeling the atmospheric signal that dominates observed radiance and must be accurately removed to retrieve ocean color (e.g., McClain 2009; Werdell et al. 2009; Siegel and Franz 2010; National Research Council 2011).

In addition to the aforementioned technical challenges, there are more fundamental limitations in the interpretation of satellite ocean color data as a biological response to climate change. Key among these is the assumption that Chl*a* is a good proxy for phytoplankton abundance (Siegel et al. 2013). Phytoplankton adjust their cellular chlorophyll content in response to environmental changes in light and nutrient availability. This physiological response can contribute an order of magnitude variability in Chl*a* and is ultimately responsible for the monthly to interannual variations in PSO anomalies. As such, changes in the satellite time series (e.g., from 2011 to 2012) can be interpreted as either a reflection of physiological variability or as absolute abundance changes, and this ambiguity has major implications for the subsequent interpretation of ocean productivity time series. This is further complicated by limitations in our ability to separate optical signals of phytoplankton abundance from colored dissolved organic matter, which is simply assumed to covary in the traditional band-ratio algorithms employed here (e.g., Siegel et al. 2013). Fully resolving these issues and thereby increasing our scientific understanding of Earth's biological response to climate change remains problematic with heritage ocean color sensors (such as MODISA and VIIRS). Moving forward will require advanced observational capabilities that expand the range of measurement wavelength (near-ultraviolet to near-infrared) and increase spectral resolution.